Fast Electromagnetic Inversion of Inhomogeneous Scatterers Embedded in Layered Media by Born Approximation and 3-D U-Net

Junping Xiao, Jiawen Li, Yanjin Chen, Feng Han, *Member, IEEE*, and Qing Huo Liu, *Fellow, IEEE*

***Abstract*— This letter presents a 3-D electromagnetic inversion method based on the Born approximation (BA) and a convolutional neural network (CNN), the 3-D U-Net. In the training stage, the BA is first used to obtain the preliminary 3-D images of a series of homogeneous scatterers with regular shapes that are further improved by the Monte Carlo method. Then, these images are used to train the 3-D U-Net. In the testing stage, inhomogeneous scatterers with complex shapes are reconstructed by both the trained 3-D U-Net and the traditional iterative method, variational Born iteration method (VBIM). Their performance is evaluated and compared.**

***Index Terms*— 3-D electromagnetic (EM) inversion, convolutional neural network (CNN), variational Born iteration method (VBIM).**

I. Introduction

ELECTROMAGNETIC (EM) inversion is to determine the model parameters of scatterers embedded in a certain region from measured field data. It has wide applications for biomedical imaging [1], airborne transient EMs [2], subsurface detection [3], and so on. In the past decades, many EM inversion methods have been developed. They are mainly divided into two categories, the noniterative approximation and rigorous iteration. The noniterative method gives the inversion results fast but only works for weak scattering scenarios. By contrast, the iterative method can be used to reconstruct the scatterers with high contrasts, although its computation cost is high. The detailed discussions of noniterative approximation and iterative methods were given in [4]. In addition, irregular and complex scatterers are more difficult to reconstruct, even when the iterative method is adopted. This is because the data equation used to solve the nonlinear inverse problem is usually underdetermined [5]. The reconstructed structure still can be distorted or the model parameters can deviate away from the true values even when the misfit between the calculated scattered field and the measured field is small.

Manuscript received July 24, 2019; revised October 7, 2019; accepted November 12, 2019. Date of publication November 27, 2019; date of current version September 25, 2020. This work was supported by the National Key R&D Program of the Ministry of Science and Technology of China under Grant 2018YFF01013300. *(Corresponding author: Feng Han.)*

J. Xiao, J. Li, Y. Chen, and F. Han are with the Institute of Electromagnetics and Acoustics, Xiamen University, Xiamen 361005, China, and also with the Key Laboratory of Electromagnetic Wave Science and Detection Technology, Xiamen University, Xiamen 361005, China (e-mail: feng.han@xmu.edu.cn).

Q. H. Liu is with the Department of Electrical and Computer Engineering, Duke University, Durham, NC 27708 USA (e-mail: qhliu@duke.edu).

Color versions of one or more of the figures in this letter are available online at http://ieeexplore.ieee.org.

Digital Object Identifier 10.1109/LGRS.2019.2953708

The EM inversion gives the model parameter distribution in the inversion domain, which is composed of several discretized cells. This is similar to a 2-D image, including discretized pixels. Inspired by this analogy, we apply the convolutional neural network (CNN) to improve the inversion results. The CNN has been successfully applied to image processing, such as object recognition [6] and image segmentation [7]. In recent work, it was applied to nonlinear EM inversion. For example, in [8], the noniterative method, backpropagation (BP), was first used to obtain the initial solutions for a nonlinear problem. They were then input into a 2-D U-Net to acquire the final dielectric model parameters in the inversion domain. In [9], a deep neural network (DNN) was used to replace the CNN to accomplish parallel computation. However, these examples are only limited to 2-D inverse problems. In this letter, we use the 3-D U-Net to perform nonlinear 3-D inversion of inhomogeneous scatterers with complex shapes. In addition, the scatterers are placed inside a layered medium that is more practical in engineering measurements compared with the homogeneous background [8], [9]. The Born approximation (BA) and Monte Carlo method (MCM) are jointly used to acquire the inputs of the 3-D U-Net. We choose BA instead of BP because BA can accommodate the low-frequency diffraction tomography and thus is more adaptable for a wide frequency range [10].

This letter is organized as follows. In Section II, we first briefly introduce the traditional iterative inversion and BA methods used to solve the nonlinear data equation. Then, the MCM used to refine the results of BA is discussed. Finally, the configuration of CNN is given in detail. In Section III, several numerical examples are presented, and the inversion results from 3-D U-Net and the traditional iterative method, variational Born iteration method (VBIM), are compared. In Section IV, conclusions are drawn and discussions are presented.

II. Theory

The Born iteration process to solve the nonlinear inverse problem includes the forward and inversion models. They are solved alternately to update the model parameters. The BA gives the model parameters directly without iteration. In strong scattering scenarios, it causes large errors. Fortunately, this shortcoming can be compensated by the 3-D U-Net.

A. Forward and Inversion Models

The forward model for EM scattering in the layered media is formulated by the state equation, which can be expressed

as [11]

$$\mathbf{E}^m_{\text{inc}} = \mathbf{E}^m_{\text{tot}} - j\omega\varepsilon_b \int_D \overline{\overline{\mathbf{G}}}^{mm}_{\mathbf{EJ}}(\mathbf{r},\mathbf{r}') \cdot \chi(\mathbf{r}')\mathbf{E}^m_{\text{tot}}(\mathbf{r}')d\mathbf{r}' \quad (1)$$

where $\chi = (\varepsilon - \varepsilon_b/\varepsilon_b)$ is the contrast function of the scatterers and ε_b is the permittivity of the background medium. The inversion model is formulated by the data equation [11], [12], which can be expressed as

$$\mathbf{E}^n_{\text{sct}}(\mathbf{r}) = j\omega\varepsilon_b \int_D \overline{\overline{\mathbf{G}}}^{nm}_{\mathbf{EJ}}(\mathbf{r},\mathbf{r}') \cdot \chi(\mathbf{r}')\mathbf{E}^m_{\text{tot}}(\mathbf{r}')d\mathbf{r}' \quad (2a)$$

$$\mathbf{H}^n_{\text{sct}}(\mathbf{r}) = j\omega\varepsilon_b \int_D \overline{\overline{\mathbf{G}}}^{nm}_{\mathbf{HJ}}(\mathbf{r},\mathbf{r}') \cdot \chi(\mathbf{r}')\mathbf{E}^m_{\text{tot}}(\mathbf{r}')d\mathbf{r}' \quad (2b)$$

where $\overline{\overline{\mathbf{G}}}^{nm}_{\mathbf{EJ}}$ and $\overline{\overline{\mathbf{G}}}^{nm}_{\mathbf{HJ}}$ are the layered medium dyadic Green's functions (DGFs) [13] connecting the equivalent electric current sources in the mth layer and the receivers in the nth layer, and D is the computation domain enclosing the scatterers and located in the mth layer.

In the forward scattering computation, (1) is discretized and $\mathbf{E}^m_{\text{tot}}$ in the mth layer is solved by the stabilized biconjugate gradient fast Fourier transform (BCGS-FFT) [14]. In the inverse scattering computation, (2) is discretized and the model parameter χ is solved by VBIM [12]. This iteration continues until the misfit between the measured scattered field and the model calculated field reaches a stop criterion. When BA is used, the forward computation is unnecessary. $\mathbf{E}^m_{\text{tot}}$ in (2) is replaced by $\mathbf{E}^m_{\text{inc}}$, and the model parameter χ is directly solved. This is much faster than the iterative scheme.

B. MCM

The BA outputs the preliminary model parameters in the inversion domain, which will be used to train or test the 3-D U-Net. The true model parameters are the outputs of the U-Net in the training stage. However, the errors of the results from BA are large for strong scenarios. Numerical results show that the model parameter distribution of scatterers tends to spread out and, thus, the outlines of the scatterers are extended. In addition, clutters exist in the inversion domain, which sometimes are erroneously judged as scatterers.

Since the BA gives the model parameter values in all the discretized cells, we can use the MCM to estimate the scatterer shape. Assume that the whole inversion domain is divided into N discretized cells. Each cell has two states, the "background" or the "scatterer." We define the probability of the "scatterer" of the ith cell as

$$P_i = \frac{|\,\varepsilon_i - \varepsilon_b\,|}{\max\limits_{1\le i\le N} |\,\varepsilon_i - \varepsilon_b\,|} \quad (3)$$

where ε_i is the model parameter in the ith cell given by BA. Obviously, a larger P_i value means that the ith cell is more like a "scatterer" cell. Therefore, we can set a threshold to label all the discretized cells in the inversion domain. The cell samples labeled as "scatterer" will cluster together and form the rough 3-D scatterer outlines although some "background" cells are also included. The cell samples labeled as "background" include both partial true "background" cells and some "clutter" cells. Their model parameters will be directly assigned as the background medium parameters. In this letter, the threshold for P_i is 7%. Although some true "background" cells cannot be filtered out by this low threshold, they may be removed by the following U-Net. Consequently, the 3-D U-Net training will be improved if the refined model parameter distribution from BA-MCM instead of BA is used as its input.

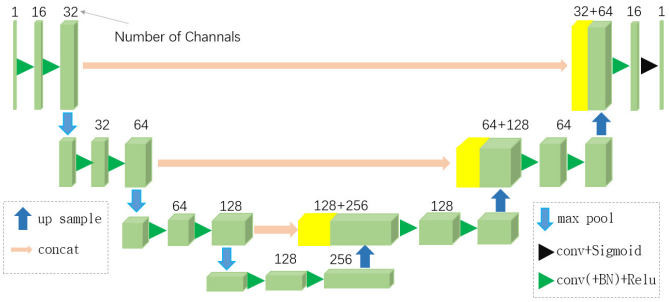

Fig. 1. Architecture of the 3-D U-Net. Its details can be found in [15].

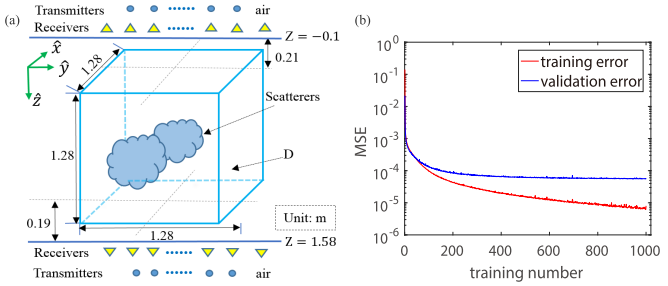

Fig. 2. 3-D U-Net training and testing for nonlinear EM inversion. (a) Inversion model has three layers. The scatterers are embedded in the middle layer. (b) Variations of errors in the training process.

C. 3-D U-Net

In this letter, we use the 3-D U-Net in [15], which is originally proposed for segmenting biomedical images. As shown in Fig. 1, the whole architecture is composed of two branches, the contracting path (left) and the expansive path (right). The contracting path extracts context information, while the expansive path provides accurate localization. Specifically speaking, in the contracting path, the main features of the images are extracted in several steps of downsampling by convolutions with different kernels. However, in the expansive path, the main features acquired in the downsampling steps are recovered for the whole image by upconvolutions. The concatenations between the layers in the contracting path and expansive path are used to compensate for the information loss in the downsampling. This is important for nonlinear EM inversion since the final reconstructed model parameters and the preliminary 3-D images from BA share common features.

The batch normalization (BN) [16] in each convolution is used to accelerate the convergence when the U-Net is trained [15]. The Relu and Sigmoid serve for nonlinear mapping. In this way, complex neural networks can approximate any nonlinear functions. Compared with the original U-Net in [15], we slightly modify its structure by reducing the number of convolution kernels so as to save training time,

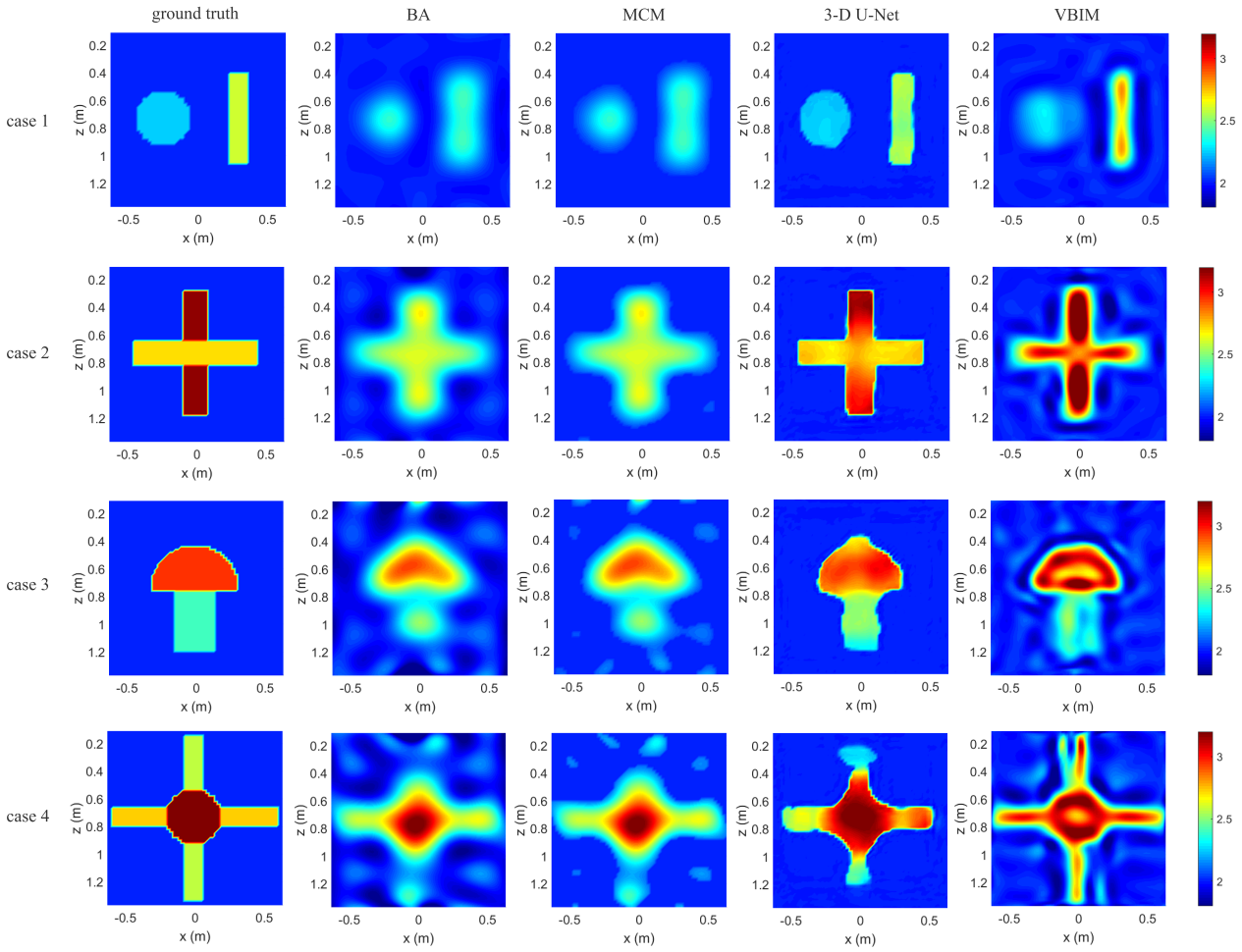

Fig. 3. Four inhomogeneous scatterers used for the 3-D U-Net testing. Only the 2-D xz slices are shown here. From the first row to the fourth row, the structures of the scatterers become more and more complicated. The first column is the ground truth, and from the second column to the fifth column, the inversion results from BA, MCM, U-Net, and VBIM are shown, respectively.

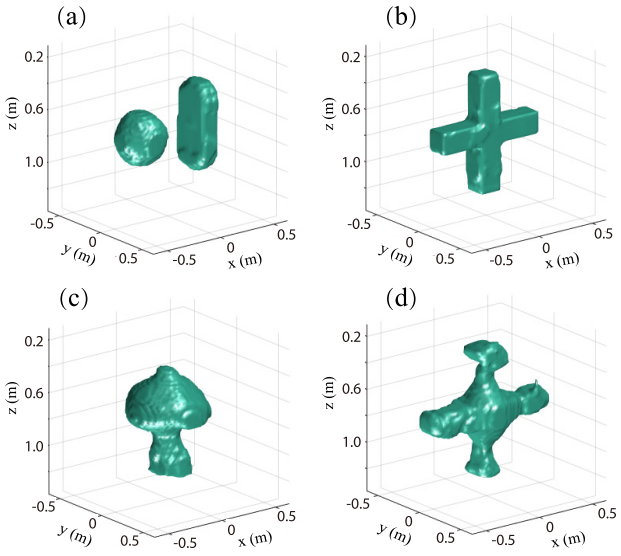

Fig. 4. 3-D isosurfaces of relative permittivity values reconstructed by U-Net. The isovalue is (a) 2.2, (b) 2.6, (c) 2.3, and (d) 2.2.

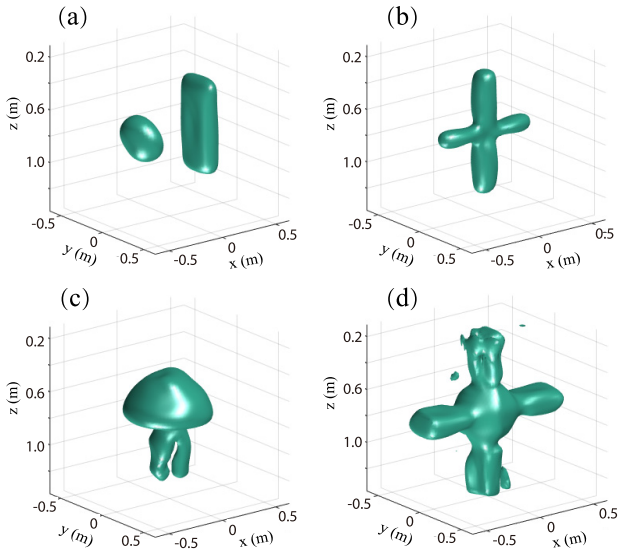

Fig. 5. 3-D isosurfaces of relative permittivity values reconstructed by VBIM. The isovalue is (a) 2.2, (b) 2.6, (c) 2.3, and (d) 2.2.

preventing overfitting and improving its generalization ability. We choose the mean square error (MSE) [17] between the input and the output of the 3-D U-Net as the cost function for training. It is defined as

$$MSE = \frac{1}{n1 \times n2 \times n3} \times \sum_{i=1}^{n1} \sum_{j=1}^{n2} \sum_{k=1}^{n3} (p'_{ijk} - p_{ijk})^2 \quad (4)$$

where $n1$, $n2$, and $n3$ are three dimensions of the image, and p'_{ijk} and p_{ijk} are the obtained and true values in each pixel.

The parameters of the 3-D U-Net will be adjusted for each training. The optimization method used in this letter is the Adam optimizer [18]. Because partial data are used to validate the U-Net after training, the MSE defined in (4) is also valid for a validation error.

III. Numerical Results

In this section, we construct the 3-D U-Net based on the deep learning framework Keras with the tensorflow support. Three groups of data sets are used. They are training data sets, validation data sets, and testing data sets. The 3-D U-Net is trained 1000 times before being used for nonlinear inversion.

A. 3-D U-Net Training

As shown in Fig. 2(a), the model has three layers. The top and bottom layers are air. The scatterers are embedded in the middle layer. The inversion domain enclosing the scatterers has the dimensions of 1.28 m $\times 1.28$ m $\times 1.28$ m, and it is divided into $64 \times 64 \times 64$ cells. The size of each cell is $\Delta x = \Delta y = \Delta z = 0.02$ m. The relative permittivity of the background medium of the middle layer is set as 2.0. There are two identical transmitter and receiver arrays. They are placed in the top and bottom layers. Each array has 5×5 transmitters and 5×5 receivers. Thus, there are totally 50 transmitters and 50 receivers, respectively. The polarization of each transmitter is (1, 1, 1). Three operating frequencies, 160, 230, and 300 MHz, are used. One of the possible applications of such a two-side and multifrequency measurement is the deep dormant tunnel detection by the cross-borehole pulse radar [19]. We construct 1700 homogeneous scatterers with four basic shapes, including cuboid, cube, sphere, and cylinder. Their dielectric constants distribute between 2.05 and 3.3 randomly. Their sizes and positions change randomly in the inversion domain. Among these 1700 data sets, 1360 sets are used for training, and 340 sets are used for validation. The measured scattered electric and magnetic field data are synthesized by the BCGS-FFT solver. The input data for the 3-D U-Net are obtained by BA and then improved by MCM. After training 1000 times in an RTX 2070 GPU which costs around 60 h, the training MSE decreases to less than 10^{-5}, as shown in Fig. 2(b). At the same time, the validation MSE becomes less than 10^{-4}. For the nonlinear EM inversion, this model misfit for the dielectric parameter is small enough [20]. This means that the U-Net after being trained 1000 times is reliable for the 3-D inversion.

B. Nonlinear Inversion by 3-D U-Net

In the testing stage, we perform the nonlinear EM inversion by the 3-D U-Net. Four inhomogeneous scatterers are reconstructed. As shown in Fig. 3, the structures of the scatterers become more and more complicated from case 1 to case 4. In case 1, the scatterers include a sphere and a cuboid which are not in touch. The radius of the sphere is 0.20 m. The dimensions of the cuboid are 0.34 m $\times$ 0.30 m $\times$ 0.66 m. The relative permittivity values are 2.25 and 2.59, respectively. A cross shape scatterer is used in case 2, which includes two perpendicular cuboids. They have the same dimensions of 0.90 m $\times$ 0.18 m $\times$ 0.18 m. However, their relative permittivity values are 2.71 and 3.16, respectively. In case 3, we use a mushroom shape to test the 3-D U-Net. The radius of the half-sphere is 0.32 m. Its relative permittivity is 2.94. The radius and height of the cylinder are 0.16 and 0.46 m, respectively. Its relative permittivity is 2.4. In case 4, four cuboids are connected to a sphere symmetrically. The sphere has a radius of 0.20 m. Its relative permittivity is 3.2. The four cuboids have the same dimensions of 0.40 m $\times$ 0.23 m $\times$ 0.14 m. However, the relative permittivity values are different. They are 2.57 for the top and bottom cuboids and 2.72 for the left and right cuboids.

Fig. 3 shows the ground truth and inversion results for four cases. We can see that BA gives the preliminary inversion results. However, both the reconstructed shapes and model parameters are far from the true values. Especially, when the scatterers are irregular, e.g., these in cases 3 and 4, the reconstructed shapes by BA are severely distorted. The major contribution of MCM is to sharpen the blurred boundaries of the scatterers and exclude clutters in the inversion domain. As a result, the 3-D U-Net has a high probability to discern the scatterer boundary and the low probability to treat these clutters as scatterers in the training stage or when executing the full-wave inversion. In other words, the shapes of the scatterers are refined by MCM before being input into the 3-D U-Net. The fourth and fifth columns in Fig. 3 show the comparisons of the 2-D xz slices reconstructed by the 3-D U-Net and VBIM. Two observations are made as follows. First, the shapes of the scatterers are better reconstructed by 3-D U-Net. The edges, corners, and boundaries of the scatterers are clearly shown in the results of U-Net. However, they are blurred in the results of VBIM. The 3-D U-Net uses the CNN to recover the model parameter distribution in the whole inversion domain from the BA-MCM results. However, $L2$-norm cost function [20] is adopted in VBIM. Nonlinear iterations are implemented to minimize the $L2$-norm cost function to obtain the parameter distribution. Consequently, the boundaries between scatterers and the background medium are blurred. Second, the retrieved model parameters by the 3-D U-Net are more accurate than those by VBIM. In cases 1–3, the model parameters from U-Net inversion match the true values well. By contrast, the reconstructed parameters from VBIM tend to show the nonuniform distribution in the scatterers. In the center region, the retrieved permittivity is larger than the true value. Because the $L2$-norm cost function results in the blurred boundary of a scatterer, the smaller equivalent current in its periphery must be compensated by the larger equivalent current in the center region to match the scattered fields measured by the receiver array. In case 4, both the U-Net and VBIM cannot reconstruct the profiles well. Although the U-Net can distinguish the distribution of permittivity values among four cuboids and the sphere, the shapes are distorted. For the results of VBIM,

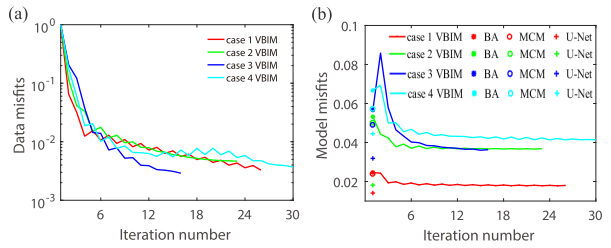

Fig. 6. Variations of data misfits and model misfits. (a) Data misfits for VBIM. (b) Model misfits for VBIM and U-Net.

the top cuboid is split into two slim bars. Figs. 4 and 5 show the 3-D isosurfaces of four scatterers by U-Net and VBIM, respectively. Clearly, the shapes of the scatterers are better reconstructed by the 3-D U-Net compared with VBIM. In addition, almost no clutter shows up in the 3-D profiles by U-Net. Fig. 6(a) shows the data misfits [20] of VBIM versus iterations in four cases. We can see that the VBIM iteration converges fastest in case 3. However, it still needs 16 iterations. Fig. 6(b) shows the variations of model misfits [20] in four cases. The model misfits decrease fast in the first few steps and then almost remain unchanged. Case 1 has the smallest final model misfit, while case 4 has the largest one. This is because the scatterer in case 1 has the simplest structure, while the scatterer in case 4 has the most complicated structure. Another interesting observation is the sudden increase in the model misfit for case 3 when VBIM is adopted. This is because the mushroom profile is complicated and the reconstructed shape may be severely distorted at the beginning although the data misfit is decreased. We also include the model misfits of the reconstructed results by BA, MCM, and U-Net in Fig. 6(b). Because only the BA takes the time, i.e., the same as the time for one-step iteration of VBIM, we put the model misfits of BA, MCM, and U-Net in Fig. 6(b) as they are recorded in the first step of VBIM iteration. The computation time cost by MCM and U-Net can be neglected compared with the time cost by BA. We can see that in four cases, BA gives the largest model misfits, while the reconstructed results by U-Net have the smallest model misfits. In cases 1–3, the final model misfits of VBIM are larger than the model misfits given by CNN. However, in case 4, they are almost the same. When the structures of the scatterers are not very complicated, the 3-D U-Net obviously outperforms the VBIM for both the computation time and the accuracy. However, when the scatterers have very complicated structures, the 3-D U-Net only has the advantage of computation time over VBIM. The accuracy is actually almost the same.

IV. Conclusion

In this letter, the BA and 3-D U-Net are combined to invert for scatterers embedded in layered media. The BA first outputs the preliminary 3-D model parameter distribution that is further refined by MCM. The 3-D U-Net is originally used for 3-D biological cell segmentation and is applied to the nonlinear EM inversion in this letter. A series of homogeneous scatterers with regular shapes is used to train the 3-D U-Net. Then, four inhomogeneous scatterers with complex shapes are input into the 3-D U-Net to carry out the fast nonlinear inversion. The comparison between 3-D U-Net inversion and the traditional VBIM method shows that the 3-D U-Net outperforms VBIM for both accuracy and efficiency. The future work will be focused on the multiparametric inversion by the 3-D U-net with multichannels, e.g., the reconstruction of arbitrary anisotropic scatterers.

References

[1] P. M. Meaney, M. W. Fanning, D. Li, S. P. Poplack, and K. D. Paulsen, "A clinical prototype for active microwave imaging of the breast," *IEEE Trans. Microw. Theory Techn.*, vol. 48, no. 11, pp. 1841–1853, Nov. 2000.

[2] B. Liang *et al.*, "A new inversion method based on distorted born iterative method for grounded electrical source airborne transient electromagnetics," *IEEE Trans. Geosci. Remote Sens.*, vol. 56, no. 2, pp. 877–887, Feb. 2018.

[3] S. Lambot, E. C. Slob, I. V. D. Bosch, B. Stockbroeckx, and M. Vanclooster, "Modeling of ground-penetrating Radar for accurate characterization of subsurface electric properties," *IEEE Trans. Geosci. Remote Sens.*, vol. 42, no. 11, pp. 2555–2568, Nov. 2004.

[4] X. Chen, *Computational Methods for Electromagnetic Inverse Scattering*. Singapore: Wiley, 2018.

[5] M. Bertero and P. Boccacci, *Introduction to Inverse Problems in Imaging*. Bristol, U.K.: IOP Publishing, 1998.

[6] A. Krizhevsky, I. Sutskever, and G. E. Hinton, "ImageNet classification with deep convolutional neural networks," in *Proc. Adv. Neural Inf. Process. Syst.*, 2012, pp. 1–9.

[7] K. He, G. Gkioxari, P. Dollár, and R. Girshick, "Mask R-CNN," in *Proc. ICCV*, Oct. 2017, pp. 2980–2988.

[8] Z. Wei and X. Chen, "Deep-learning schemes for full-wave nonlinear inverse scattering problems," *IEEE Trans. Geosci. Remote Sens.*, vol. 57, no. 4, pp. 1849–1860, Apr. 2019.

[9] L. Li, L. G. Wang, F. L. Teixeira, C. Liu, A. Nehorai, and T. J. Cui, "DeepNIS: Deep neural network for nonlinear electromagnetic inverse scattering," *IEEE Trans. Antennas Propag.*, vol. 67, no. 3, pp. 1819–1825, Mar. 2019.

[10] W. C. Chew, *Waves and Fields in Inhomogeneous Media*. New York, NY, USA: IEEE, 1995, ch. 9.

[11] Y. Chen, P. Wen, F. Han, N. Liu, H. Liu, and Q. H. Liu, "Three-dimensional reconstruction of objects embedded in spherically layered media using variational Born iterative method," *IEEE Geosci. Remote Sens. Lett.*, vol. 14, no. 7, pp. 1037–1041, Jul. 2017.

[12] W. Zhang and Q. H. Liu, "Three-dimensional scattering and inverse scattering from objects with simultaneous permittivity and permeability contrasts," *IEEE Trans. Geosci. Remote Sens.*, vol. 53, no. 1, pp. 429–439, Jan. 2015.

[13] K. A. Michalski and J. R. Mosig, "Multilayered media Green's functions in integral equation formulations," *IEEE Trans. Antennas Propag.*, vol. 45, no. 3, pp. 508–519, Mar. 1997.

[14] F. Han, J. L. Zhuo, N. Liu, Y. Liu, H. Liu, and Q. H. Liu, "Fast solution of electromagnetic scattering for 3-D inhomogeneous anisotropic objects embedded in layered uniaxial media by the BCGS-FFT method," *IEEE Trans. Antennas Propag.*, vol. 67, no. 3, pp. 1748–1759, Mar. 2019.

[15] Ö. Çiçek, A. Abdulkadir, S. S. Lienkamp, T. Brox, and O. Ronneberger, "3D U-Net: Learning dense volumetric segmentation from sparse annotation," in *Proc. Int. Conf. Med. Image Comput. Comput.-Assist. Intervent. (MICCAI)*. Cham, Switzerland: Springer, 2016, pp. 424–432.

[16] S. Ioffe and C. Szegedy, "Batch normalization: Accelerating deep network training by reducing internal covariate shift," in *Proc. 32nd Int. Conf. Int. Conf. Mach. Learn.*, 2015, pp. 448–456.

[17] S.-W. Fu, T.-W. Wang, Y. Tsao, X. Lu, and H. Kawai, "End-to-end waveform utterance enhancement for direct evaluation metrics optimization by fully convolutional neural networks," *IEEE/ACM Trans. Audio, Speech, Language Process.*, vol. 26, no. 9, pp. 1570–1584, Sep. 2018.

[18] D. P. Kingma and J. Ba, "Adam: A method for stochastic optimization," 2014, *arXiv:1412.6980*. [Online]. Available: https://arxiv.org/abs/1412.6980

[19] S.-W. Kim, S.-Y. Kim, and S. Nam, "Short-time Fourier transform of deeply located tunnel signatures measured by cross-borehole pulse radar," *IEEE Geosci. Remote Sens. Lett.*, vol. 8, no. 3, pp. 493–496, May 2011.

[20] T. Lan, H. Liu, N. Liu, J. Li, F. Han, and Q. H. Liu, "Joint inversion of electromagnetic and seismic data based on structural constraints using variational born iteration method," *IEEE Trans. Geosci. Remote Sens.*, vol. 56, no. 1, pp. 436–445, Jan. 2018.